Synthesis and Characterization of Gold@Gold(I)−Thiomalate Core@Shell Nanoparticles

Gastón Corthey,[†] Lisandro J. Giovanetti,[†] José M. Ramallo-López,[†] Eugenia Zelaya,[‡] Aldo A. Rubert,[†] Guillermo A. Benitez,[†] Félix G. Requejo,[†] Mariano H. Fonticelli,[†,*] and Roberto C. Salvarezza[†]

[†]Instituto de Investigaciones Fisicoquímicas Teóricas y Aplicadas (INIFTA), Universidad Nacional de La Plata-CONICET, Sucursal 4 Casilla de Correo 16 (1900) La Plata, Argentina, and [‡]Centro Atómico Bariloche, Comisión Nacional de Energía Atómica-CONICET. Av. Bustillo 9500, Bariloche, 8400 Rio Negro, Argentina

ABSTRACT In this paper, the synthesis of gold@gold(I)−thiolate core@shell nanoparticles is described for the first time. The chemical nature and structure of these nanoparticles were characterized by a multi-technique approach. The prepared particles consist of gold metallic cores, about 1 nm in size, surrounded by stable gold(I)−thiomalate shells (Au@Au(I)−TM). These nanoparticles could be useful in medicine due to the interesting properties that gold(I)−thiomalate has against rheumatoid arthritis. Furthermore, the described results give new insights in the synthesis and characterization of metallic and core@shell nanoparticles.

Gold nanoparticles are widely studied because they exhibit extraordinary properties that might have strong impact in different science and technology fields.[1−3] The interest in these fascinating nanostructures covers a wide range of specific areas, as heterogeneous catalysis, optics, sensitive analysis, or medicine. In particular, because of their small dimensions, they can pass through a cellular membrane and be incorporated into biological systems. Metal nanoparticles can be conjugated with small molecules for biomolecular targeting or recognition ligands allowing molecular specificity.

Thiols are particularly important in the synthesis and applications of gold nanoparticles. In fact, these molecules allow a precise control of the particle size by tuning the hydrocarbon chain length and gold/thiol concentration ratio.[4,5]

While it is easy to prepare stable thiol monolayer-protected nanoparticles soluble in organic solvents (by using standard procedures such as the Brust−Schiffrin two-phase method),[6] isolable, stable, and water-soluble thiolate-protected gold nanoparticles are more difficult to prepare. Water-soluble gold nanoparticles can be used in diagnostics, bioelectronic devices, and targeted drug delivery.[2,7]

For the synthesis of this kind of nanoparticles, several parameters have to be precisely controlled, such as pH solution, solvent composition, and the thiol terminal group. Certainly, there are many reports where nearly monodisperse water-soluble gold nanoparticles have been prepared, under different conditions and using various thiols.[8−22] Moreover, structural studies of thiolate monolayer-protected water-soluble nanoparticles have been recently published by the group of Ko-

rnberg:[8] using X-ray diffraction (XRD), they studied p-mercaptobenzoic acid protected gold nanoparticles [$Au_{102}(MBA)_{44}$]. Later, theoretical studies on these nanoparticles by Häkkinen,[23] Galli,[24] Jiang,[25] and co-workers appeared. They proposed a structure of gold atoms in a metallic core protected by a Au(I)−thiolate shell, in a configuration they called "staple" motifs. The topic of the actual structure of thiols on gold surfaces is a matter of active discussion nowadays.[26]

Other kinds of gold nanoparticles protected by thiols with carboxylic acids were synthesized by Chen and Kimura.[9] In this synthetic route, which has attracted considerable attention,[10,27,28] they used thiomalic acid (TMA, also known as mercaptosuccinic acid, MSA) as capping agent and sodium borohydride (NaBH₄) as reductant. When TMA is used as both reductant and protecting agent, the resulting particles are efficiently stabilized against aggregation when this thiol is used in 40% concentration and above.[29] However, when the TMA/Au(III) ratio is higher than 1, no particle formation is observed.[29] Hence, different phenomena regarding their formation and growth should be understood. As did Chen and Kimura,[9] Ackerson et al.[10] used the same TMA/Au molar ratio (2.5), with equimolar NaBH₄ to
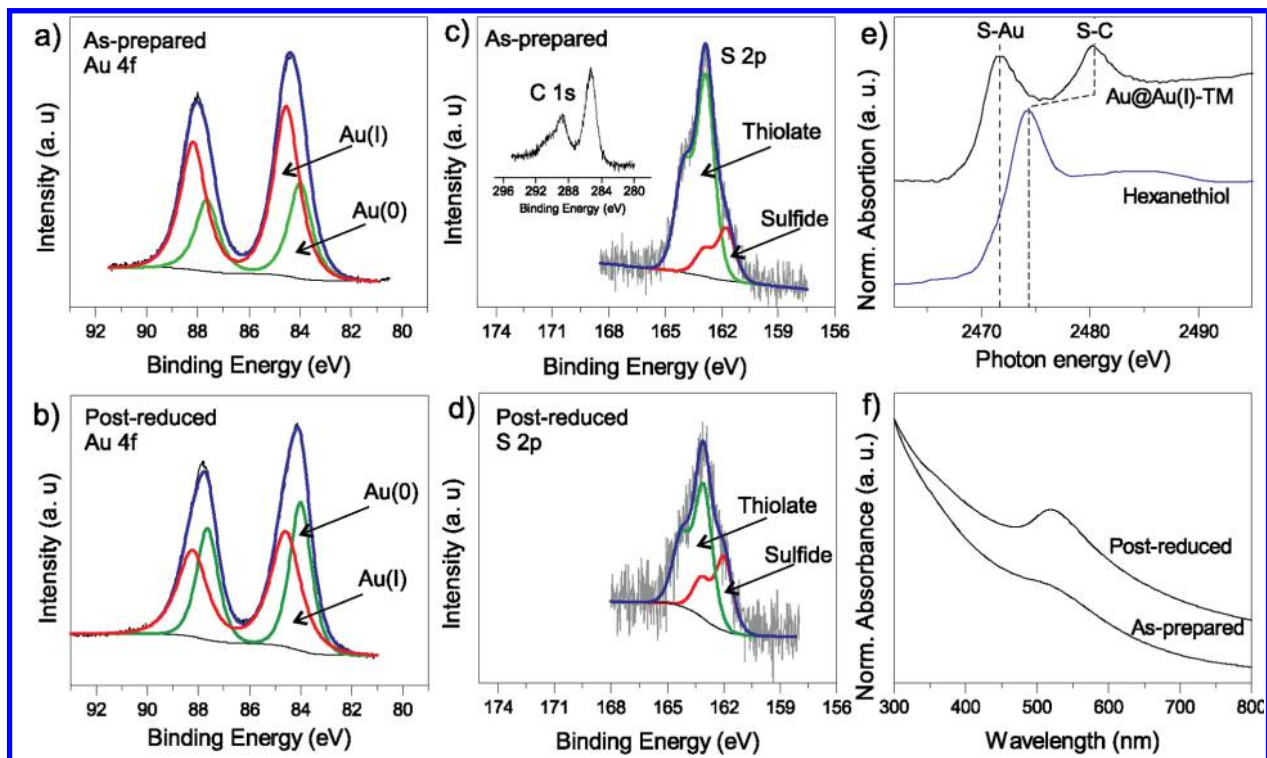
Figure 1. Au 4f XPS signals of the as-prepared (a) and post-reduced (b) Au@Au(I)−TM nanoparticles. S 2p signals of the as-prepared (c) and post-reduced (d) Au@Au(I)−TM nanoparticles. Inset in c: C 1s signal. (e) S K-edge XANES spectra of Au@Au(I)−TM nanoparticles and hexanethiol. The lower spectrum corresponds to S K-edge XANES signal for unbound (free) thiols. (f) UV/vis spectra of the as-prepared and post-reduced nanoparticles.

HAuCl₄. In that work, an incomplete gold reduction has been observed, although the nature of the resulting products has not still been reported.

In the present work, we have focused on the particular synthetic conditions of TMA-capped gold nanoparticles, where incomplete reduction takes place. The chemical nature and structure of the synthesis products were characterized by using a multi-technique approach: X-ray photoelectron spectroscopy (XPS), transmission electron microscopy (TEM), high-resolution TEM (HRTEM), small-angle X-ray scattering (SAXS), extended X-ray absorption fine structure (EXAFS), X-ray absorption near-edge structure (XANES), and UV−vis spectroscopy (UV/vis). We were able to demonstrate that under conditions of incomplete reduction the TMA-capped gold nanoparticle synthesis results in the formation of gold core−gold(I)−thiomalate shell nanoparticles (Au@Au(I)−TM).

Whereas the Au(I)−thiolate complex is an intermediate product in the synthesis of thiolate-protected gold nanoparticles[6,11,12,30,31] and it has been proposed as the real molecular cap of those nanoparticles,[8,23,24] in our best knowledge, the synthesis of Au@Au(I)−thiolate core@shell nanoparticles (where the Au(I)−thiolate arrays in a multilayer shell) has not been reported. The case of thiomalate is particularly interesting as the highly soluble Au(I)−TM complexes have a wide range of applications in medicine: treatment of rheumatoid arthritis,[32] antitumor,[33] and anti-

HIV activity.[34] It is known that Au(I)−TM inhibits the expression of molecules involved in cell adhesion and neutrophil adherence to endothelial cells,[35−37] and that these effects may contribute to its strong anti-inflammatory activity. However, the toxicity of the complex has limited their use seriously. On the other hand, the presence of carboxylate groups, which are susceptible to covalent modification, in the Au(I)−TM nanoparticles' stable shell could open interesting possibilities for cell targeting and slow drug delivery.[38]

RESULTS AND DISCUSSION

Au@Au(I)−TM nanoparticles were synthesized by a modified Brust method,[39] developed by Chen and Kimura.[9] The obtained product was a dark-brown solid powder which was easily dispersed in water. Different TMA/Au molar ratios (12.5:1, 2.5:1, and 0.5:1) were tested. In the case of the lowest TMA/Au value, some aggregation was inferred from the UV−vis spectrum. For this reason, the results showed below refer to the higher molar ratios (TMA/Au = 2.5:1 and 12.5:1), particularly TMA/Au = 2.5:1.

For the XPS characterization, a portion of the powder was dispersed in ethanol and drop cast on a Pt foil. The Au 4f signal (Figure 1a) shows that the Au(0) contribution (84.0 eV) was only 30% of the overall signal, while the 70% corresponds to Au(I) (84.5 eV).[40] Interestingly, the S(total)/Au(I) ratio was about 1. This means that there is a 1:1 correspondence between the num-

ber of sulfur and Au(I) species. Accordingly, the total Au amount, which includes both Au(I) and Au(0), is greater than that of sulfur. The assignment of the component at 84.5 eV to Au(I)−TM species is supported by previous XPS data of Au(I)−thiolate complexes.[40] It is worth noting that XPS spectra for dodecanethiolate monolayer-capped Au nanoparticles (1.6 nm in diameter) also exhibit a low intensity Au 4f component 0.36 eV positively shifted with respect to the clean Au signal.[41] Although this component has been assigned to final state effects,[42,43] in our case, final state effects cannot justify the strong intensity and the 0.5 eV binding energy shift observed in the spectra (Figure 1a). We have also observed that the C 1s signal is consistent with the presence of carboxylate groups from the TMA (inset in Figure 1c).[44,45]

The XPS S 2p spectrum shown in Figure 1c was well fitted considering two components which were found at 162.9 and 161.8 eV. The binding energy of 162.9 eV is higher than the one observed for thiols adsorbed on Au in thiolate-protected Au nanoparticles (162.0−162.5 eV).[40] This is in accordance with the presence of Au−S bonds in a Au(I)−thiolate compound, where bridging sulfur [Au−S(R)−Au−S(R)] is present. The shift to a higher binding energy can be explained by a reduction in the negative charge in sulfur, with respect to the one observed for sulfur chemisorbed on Au.[40,46] The component at 161.8 eV has been assigned to sulfide species.[47] The thiolate component contribution is 80% of the total signal, while sulfide accounts for the remaining 20%. No traces of oxidized S, such as sulfonates, were detected since no signals were observed at higher binding energies (>167 eV).[48,49]

The presence of unbound TMA molecules was discarded considering the XANES spectra at the S *K*-edge region (Figure 1e). Indeed, the spectrum for the dark-brown powder, which shows two peaks separated by about 7 eV, is characteristic of thiolate-metal bonds. The peak at lower energy has been assigned to excitations into the S−Au bond. This peak was not observed when free thiols or nanoparticles with considerable amounts of unbound thiols were studied by XANES.[50−53] The second peak corresponds to excitations into the S−C bond, centered at a higher energy with respect to that observed for unbound alkylthiols (see Figure 1e, lower spectrum), and reflecting the formation of the S−Au bond as part of the major chemical species.[51,52] It is worth noting that independently of the metal used the same two peaks were observed.[53] It is also important to consider that, if unbound TMA was present in a considerable extent, a similar signal to that found for hexanethiol should be obtained. Certainly, as the peak for hexanethiol is only related to excitations into the S−C states, its shape is expected to be independent of the thiol employed.[51,52]

As already has been reported, Au(III) was not completely reduced for the current TMA/Au proportion.[10]

The prominent resistance of Au(I)−TM toward reduction was confirmed by performing Au electrodeposition on highly oriented pyrolitic graphite (HOPG) from a TMA/HAuCl$_4$ solution, comparing the data with those obtained with a HAuCl$_4$ solution (without TMA). While a high negative current due to Au electrodeposition was obtained in the latter case, no appreciable reduction was observed with the former solution (see Supporting Information). Furthermore, potential excursions to very negative potentials—into the hydrogen evolution reaction region—did not allow Au(I)−TM reduction. In order to further reduce the obtained Au(I) species in the as-prepared nanoparticles, a post-reduction process was carried out adding a NaBH$_4$ excess to a portion of the Au@Au(I)−TM nanoparticles dispersed in water. It is worth noting that the post-reduction did not successfully reduce the Au(I)−TM complex. However, Au(I) was reduced to some extent [Au(0)/Au(I) ratio increased], and the S(total)/Au(total) ratio decreased after the borohydride treatment (Figure 1b,d).

The UV/visible spectrum of the product dispersed in water (Figure 1f) exhibits a small plasmon peak at 520 nm, with a characteristic intensity of gold nanoparticle samples which contain cores of approximately 2 nm.[4,9] It is interesting to note that the post-reduction process produces an increase in the peak intensity, which indicates a larger size of gold cores. On the other hand, the plasmon peak remains in the same position, which rules out nanoparticle core aggregation. The UV/vis spectra of the different reagents and reference materials used in the particle preparation are included in the Supporting Information.

As a logical consequence from the data discussed above, the dark-brown powder must be composed of small gold nanoparticles, Au(I)−TM, and sulfur species, where both Au−S and S−C bonds are present. Interestingly, if the structure of the as-prepared nanoparticles was that of thiolate-protected nanoparticles with a metallic core surrounded by a Au(I)−TM monolayer, a post-reduction treatment would have caused no effect on the nanoparticles, leading to the same XPS and UV/vis spectra.

Afterward, EXAFS, SAXS, and TEM results were used to characterize the nanoparticle geometry and structure. In order to discard the possibility that Au(I) species were bonded to the carboxylate group, oxygen was first used to fit the low distance contribution of the EXAFS spectrum (Figure 2). However, in this case, the fit was not good and distance was higher than that expected for Au−O bonds (between 0.193 and 0.207 nm).[54,55] In contrast, a shell of sulfur atoms fitted data very well, leading to Au−S distances of 0.231 nm, in good agreement with Au−S distance of 0.2289,[56] 0.230,[57] and 0.237 nm,[58] previously reported for Au(I)−TM and those observed experimentally[8] and estimated from theoretical calculations[23,24] for the RS−Au−RS "staple" motifs, which are believed to cover
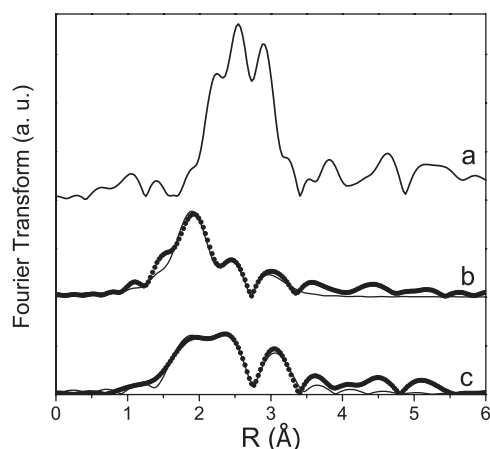
Figure 2. Fourier transforms of Au L_3 edge EXAFS spectra of (a) Au foil, (b) Au@Au(I)−TM nanoparticles, and (c) post-reduced Au@Au(I)−TM nanoparticles. Solid lines on curves b and c show the EXAFS fits.

the Au cores in thiolate monolayer-protected Au nanoparticles. A contribution from a second Au shell was also considered to fit the 0.14−0.35 nm region, which is associated with the Au−Au distances of the Au core. These results are in accordance with the two components observed in the XPS Au 4f signal.
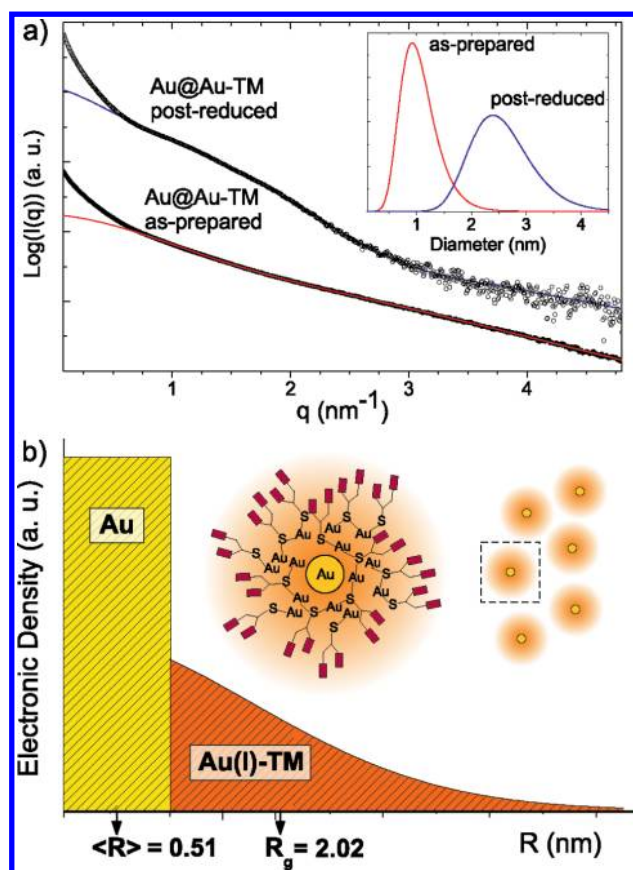

Figure 3. (a) SAXS data for Au@Au(I)−TM and Au@Au(I)−TM post-reduced and the fitting curves in red and blue, respectively. The obtained distributions for core size from the fitting routine are shown in the top right corner. (b) Scheme of the electronic density proposed to fit the SAXS data.

TABLE 1. Results of EXAFS Signal Fitting[a]

	pair	N	R (nm)	σ^2 (nm^{-2})
Au@Au(I)−TM as-prepared	Au−S	1.2(3)	0.231(3)	0.00005(1)
	Au−Au	4.4(8)	0.283(3)	0.0005(1)
Au@Au(I)−TM post-reduction	Au−S	0.6(2)	0.231(3)	0.000030(5)
	Au−Au	6.5(8)	0.284(5)	0.00011(5)

[a]Coordination number (N), bond distance (R), and Debye−Waller factor (σ^2) obtained for Au@Au(I)−TM nanoparticles before and after post-reduction.

It is well-known that, for small metallic nanoparticles (smaller than 5 nm diameter), the metal−metal average coordination number (N) can be used to estimate the size of the particle if some assumptions over their shape are made.[59−61] For spherical nanoparticles, N decreases as the particle size decreases, up to a limit value of 5.53, which is the average N for an ideal Au_{13} cuboctahedron. In our case, we obtained a lower value (N ≈ 4.4), which is an indication that not only metallic Au is present but also another different Au phase must be present to explain such small N value. A metallic phase and a second phase with sulfur atoms in the first coordination sphere for Au(I) species can reproduce this result. While Au atoms inside the metallic phase are surrounded by another 12 Au atoms, Au species in the second phase would contribute with zero to the Au−Au coordination number. Therefore, we can conclude that these nanoparticles mainly consist of Au(I)−TM with some Au(I)−sulfide and a small amount of metallic Au. After the post-reduction treatment, a decrease in the Au−S coordination number as well as an increase in the Au−Au coordination number was observed (Table 1). These changes indicate that the metallic Au(0) amount increased at the expense of the Au(I) species. Furthermore, while the S(total)/Au(total) ratio estimated from XPS data decreased as a consequence of the post-reduction treatment, the Au−S distance did not change. The high Debye−Waller factor obtained for the Au shell is in accordance with previous results for small metallic nanoparticles.[59] Additionally, density functional theory studies have shown that very small thiolate-capped Au nanoparticles have a very disordered structure, consistent with the Debye−Waller factors for the nanoparticles fitted here.[23,24,62,25]

After having established the chemical nature of the two domains present in the material, the distribution, and geometrical arrangement of Au(0) and Au(I)−TM species was inferred from SAXS measurements. The obtained SAXS curves for the powder dispersed in water and the same product after post-reduction are shown in Figure 3a. The better curve fitting was obtained proposing a two-electron density model: a constant density attributed to the Au(0) core and a Gaussian electronic density distribution for a shell associated with the Au(I)−TM layer. A log normal distribution[63] for the radius of the Au(0) core was introduced in the fitting routine to take into account the size dispersion. The ob-

TABLE 2. Fitting Routine Parameters from SAXS Analysis[a]

	$\langle R \rangle$ (nm)	d (nm)	R_g Au(I)—TM (nm)
Au@Au(I)—TM as-prepared	0.51(2)	0.069(8)	2.02(4)
Au@Au(I)—TM post-reduction	1.26(1)	0.119(5)	3.9(3)

[a]The obtained values for the average radius ($\langle R \rangle = e^{\ln(\mu) + \nu^2/2}$) and the size distribution standard deviation ($d = ((e^{\nu^2} - 1)e^{2\ln(\mu) + \nu^2})^{1/2}$) calculated from the log normal distribution ($(1/(2\pi)^{1/2}\nu r)\exp[(-(\ln(r) - \ln(\mu))^2)/(2\nu^2)])$) and the gyration radius (R_g) of the Au(I)—TM shell are shown.

tained values for the different parameters are shown in Table 2.

The fit function describes very accurately the experimental data in the high q region (0.85 to 5 nm^{-1}). This result indicates that the product synthesized with TMA/Au = 2.5 is formed by nanoparticles consisting of a Au(0) core and Au(I)—TM shell (Au@Au(I)—TM), discarding the possibility of Au cores immersed in a bulk Au(I)—TM polymer. The deviation from the experimental data in the low q region could be attributed to the formation of aggregates of Au@Au(I)—TM particles. This aggregation mechanism, if present, does not change significantly during the post-reduction treatment and may be attributed to the formation of small oligomers[56] that interconnect the nanoparticles in a non-unique way. This model indicates that the as-prepared Au@Au(I)—TM nanoparticles have Au cores with an average radius of 0.51(2) nm, which increases up to 1.25(1) nm as a consequence of the post-reduction process. Furthermore, these results are in good agreement with those reported by Chen and Kimura.[9] These authors have found an average core diameter of 1.02 nm by XRD experiments when a 2.5:1 TMA/Au molar ratio was employed. The SAXS data are in consonance with the reported data but also show that the cores are surrounded by a multilayer Au(I)—TM shell. This model is also compatible with the EXAFS results and explains the presence of the attenuated plasmon resonance peak at the UV/vis curves for the Au@Au(I)—TM nanoparticles in water and the increase in the intensity of the plasmon after the post-reduction process.

The Au@Au(I)—TM nanoparticles were also characterized by TEM. A bright-field (BF) image of the nanoparticles is shown in Figure 4a. Surprisingly, the mean diameter obtained was 3.7 ± 1.3 nm (see Supporting Information for the histogram), which is higher than the

one obtained by SAXS (Figure 3a and Table 2) and that expected from the UV/vis spectrum (Figure 1d). However, this can be explained considering the proposed Au@Au(I)—TM structure. In fact, Kim et al. synthesized gold nanoparticles irradiating a Au(I)—alkanethiolate—the precursor of Brust synthesis—with a TEM electron beam.[64] Therefore, the Au(I) of the Au(I)—TM shell of the as-prepared particles can be reduced by the electron beam of the TEM, incrementing the size of the metallic Au core. Hence, the size determined by TEM is related to the metallic Au coming from both the metallic cores originally synthesized and also the metallic Au generated by reduction of Au(I) by the electron beam. This result is consistent with the diameter observed by the group of Kimura, who have used a TMA/Au ratio of 3:1.[65] In that paper, they reported a diameter obtained by TEM of 3.4 ± 0.8 nm, larger than the one they obtained earlier by XRD (1.02 nm) when a 2.5:1 TMA/Au ratio was employed.[9] These results suggest that special care should be taken when measuring the size of metal nanoparticles: it is crucial to combine local techniques with average ones in order to avoid miss estimation of their size. It is worth noting that SAXS measurements were carried out using a water dispersion of the synthesized material. In this arrangement, nanoparticles of every size contribute to the signal.

Although it is not representative of the whole system, some larger particles not detected by SAXS have been observed by TEM (Figure 4b). This is not contradictory since SAXS experiments were performed on liquid samples and a ripening process can be produced by electron bombardment after the deposition of particles on a solid substrate during TEM experiments.[66]

HRTEM images were taken along [110] zone axis of the Au fcc cell. A nanoparticle with crystalline structure is observed in the image (Figure 4c), which confirms the presence of metallic Au in the whole particle. The HRTEM images were compared with the simulations of truncated octahedron nanoparticles over an amorphous carbon layer using jEMS software. The best fit to a particle with 1238 atoms is shown in Figure 4d (see Supporting Information for more details).

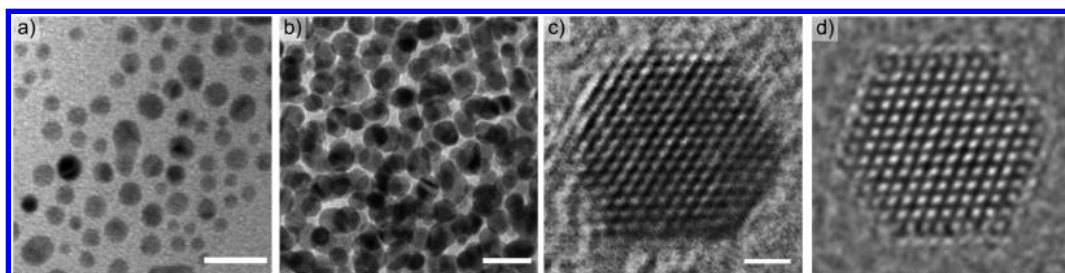Selected area electron diffraction (SAED) experiments and dark-field (DF) images also confirm the crys-

Figure 4. (a) Bright-field image of the characteristic Au@Au(I)—TM nanoparticles. Scale bar = 10 nm. (b) Bright-field image of the small population of larger nanoparticles. Scale bar = 20 nm. (c) HRTEM image of as-prepared Au@Au(I)—TM nanoparticles. Scale bar = 1 nm. (d) Simulated HRTEM image of a truncated octahedron of 1238 atoms, defocus value = 145 nm.

1) $HAuCl_4 + 3\ RSH \longrightarrow Au(I)\text{-}SR + RS\text{-}SR + 4\ HCl$

2) $n\ [Au(I)\text{-}SR] \longrightarrow [Au(I)\text{-}SR]_n$ (Oligomer)

3) $HAuCl_4 + [Au(I)\text{-}SR]_n \xrightarrow{\ NaBH_4\ }$ Au@Au(I)-SR nanoparticles

RSH =

Au(I)-SR =
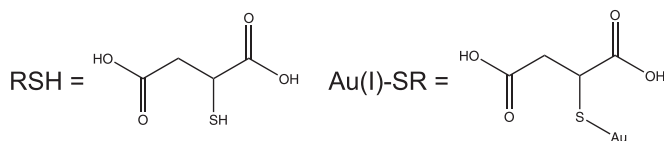
Scheme 1. Possible reactions involved in the nanoparticle synthesis.

talline structure of the nanoparticles (see Supporting Information).

It has already been stated that Au(I)−thiolate polymeric species are the precursors in many thiolate-protected nanoparticles synthetic routes.[6,11,12,30,31] Certainly, the reduction of the Au(I) polymer by $NaBH_4$ led to the formation of the metallic Au nanoparticles. However, a more complex scenario for the Au(I)−TM has to be considered. It is argued that in the Au(I)−TM case nucleation of Au clusters takes place in the solution containing a Au(I)−TM-like polymer. This polymer can gradually cover the growing Au clusters, finally blocking completely their growth.

In contrast to the commonly observed behavior of Au(I)−thiolate toward $NaBH_4$ reduction, in the current case no complete reduction of the Au(I)−TM could be obtained, even with a post-reduction procedure, originating gold-core Au(I)−TM-shell nanoparticles. Also in the case of TMA/Au = 12.5 molar ratio, an incomplete reduction of gold was observed, as the XPS and UV/vis results indicate. It is remarkable to notice that $NaBH_4$ does not allow a complete reduction of oxidized Au, even when it is used in a 10-fold excess. Both the aqueous $NaBH_4$ and the electrochemical polarization provide enough driving force for the Au(I) reduction, although it is forming a stable complex (see Supporting Information for details). Then, a kinetic hindrance, which is the motivation of further studies, might be the responsible for the partial Au(I) reduction.

Moreover, the nature of the particular thiol, TMA, or the solvent used might play a crucial role since Au(I)−alkanethiolates are known to be reduced by $NaBH_4$ in organic solvents.[30,31] Nonetheless, the presence of a Au(I)−dodecanethiolate species has been found in a nonaqueous medium, which has been attributed to either an incomplete reduction during the synthesis or to sample degradation.[59] Hence, although the above discussion strictly applies to the Au(I)−TM system, it could illuminate more general phenomena that have not yet been well understood.

In a plausible reaction scheme (Scheme 1), the Au precursor ($HAuCl_4$) is reduced by TMA, producing Au(I)−TM oligomers (steps 1 and 2).[30,11] As TMA is added in defect with respect to $HAuCl_4$ (considering

the 3:1 stoichiometric relation), some $HAuCl_4$ remain in excess.[31] Then, this reactant and the Au(I)−TM produced in steps 1 and 2 react with $NaBH_4$ to form the Au@Au(I)−TM nanoparticles already described. Shon *et al.* reported that the reducing agent causes fragmentation of the Au(I) intermediate *en route* to gold nanoparticles.[67] Furthermore, it was stated that there is a complete breakup of the Au(I)−thiolate species upon addition of $NaBH_4$ to the reaction mixture. Then, it is not yet clear whether the observed kinetic hindrance is simply related to the nanoparticle passivation by the polymer layer or if it is also connected to a low rate of the polymer decomposition upon $NaBH_4$ addition.

The final products obtained in both systems (the as-prepared and the post-reduced Au@Au(I)−TM nanoparticles) could be seen as intermediates in the synthesis of thiolate monolayer-protected metallic nanoparticles that, somehow, were not able to be fully reduced. In this regard, the possibility of partially reducing the Au(I) by carrying out the post-reduction indicates that the Au@Au(I)−TM nanoparticles are not a thermodynamically stable product when $NaBH_4$ is used. Therefore, a complete reduction of the Au@Au(I)−TM nanoparticles would lead to thiolate monolayer-protected gold nanoparticles. In the current case, as an incomplete reduction of Au(I) was achieved, the metallic gold core is surrounded by a multilayer Au(I)−TM shell. As already stated, the Au−S bond length observed from the EXAFS data of Au@Au(I)−TM nanoparticles (0.231 nm) agrees with that in the RS−Au−RS "staple" motifs recently proposed[8] and with the Au−S distance reported for Au(I)−TM polymers.[57,58,68] From the above proposed reaction scheme, it could be claimed that the Au(I)−RS oligomers are the precursors of the motifs observed at the surface of thiolate-covered gold nanoparticles. However, as a thick Au(I)−TM layer covers the Au cores, it is not possible from our data to propose a structure for the interface between metallic Au and Au(I)−TM.

With regard to Au@Au(I)−TM nanoparticle stability in aqueous media, the as-prepared material was stored for 7 months dispersed in water at 4 °C, and XPS experiments were performed to test the chemical state of the nanoparticles. The Au(I)/Au(0) ratio remains equal to the as-prepared particles while only 20% of the sulfur was found to be oxidized (see Supporting Information).

CONCLUSION

In summary, the synthesis and characterization of core@shell nanoparticles composed by a metallic Au core and a multilayer thiolate shell has been described. Although the used thiol was TMA, the appropriate conditions might be found to synthesize other Au core/thiolate shell nanoparticles. These particles are very stable in water, observing only little degradation after several months. On the other hand, the prepared

Au@Au(I)−TM nanoparticles have potential use in medicine: these particles might be used as Au(I)−TM complex carriers in order to deliver them to desired places, diminishing the high toxicity of this compound.

Finally, the importance of attacking these kinds of systems with a multi-technique approach to avoid misunderstanding of some properties of the nanoparticles such as the size obtained by TEM has been shown.

METHODS

Synthesis of Au@Au(I)−TM Nanoparticles. $HAuCl_4$ was prepared by dissolving a gold wire (99.9%) in aqua regia following the protocol described elsewhere.[69] An aqueous solution containing 2.54×10^{-2} M $HAuCl_4$ was prepared. In a typical nanoparticle synthesis where the TMA/Au molar ratio of 2.5 was used, 19.7 mL (0.50 mmol) of the $HAuCl_4$ solution was added to an Erlenmeyer and stirred with 100 mL of methanol. Then, 0.180 g (1.25 mmol) of thiomalic acid (TMA Fluka, 99%) was added to the $HAuCl_4$ solution. The mixture was stirred for 5 min, and the solution turned to light yellow, with a pH of 1.7. Then, 10 mL of 2% aqueous solution of $NaBH_4$ (5 mmol) (Fluka, 96%) was added. The pH of the solution increased to over 8. The solution turned dark brown immediately, and a solid was obtained. The mixture was further stirred for 1 h. The precipitate was washed two times with a 80% methanol and 20% water mixture by centrifugation and ultrasonic redispersion routine to remove inorganic impurities (sodium, chloride, and boron species) and three times with methanol to remove unbound TMA. Finally, the nanoparticles were resuspended in ethanol and dried under nitrogen flow. The obtained product was easily dispersed in water.

Post-reduction of Au@Au(I)−TM Nanoparticles. In order to further reduce the obtained Au(I) species, a post-reduction process was carried out. Fifty milligrams of the washed nanoparticles was placed in contact with 100 mg of $NaBH_4$ for 20 min and washed with methanol.

General Methods. X-ray photoelectron spectroscopy (XPS) was performed using a Mg Kα source (XR50, Specs GmbH) and a hemispherical electron energy analyzer (PHOIBOS 100, Specs GmbH). A two-point calibration of the energy scale was performed using sputtered cleaned gold (Au $4f_{7/2}$, binding energy (BE) = 84.00 eV) and copper (Cu $2p_{3/2}$, BE = 933.67 eV) samples. For spectra deconvolution of the S 2p and Au 4f region, a Shirley-type background was subtracted and a combination of Lorentianz and Gaussian functions was used. In the case of S 2p, the full width at half-maximum (fwhm) was fixed at 1.1 eV, and the spin−orbit doublet separation of S $2p_{3/2}$ and S $2p_{1/2}$ signal was set to 1.18 eV. The BEs and peak areas were optimized to achieve the best adjustment. For Au 4f region, the fwhm of the peaks was set to 1.0 eV, and the spin−orbit doublet separation of Au $4f_{5/2}$ and Au $4f_{7/2}$ was set to 3.65 eV. Sulfur to gold ratio was estimated by the measurement of the areas of Au 4f and S 2p signals corrected by the relative sensitivity factor (RSF) of the elements. XPS of the Au@Au(I)−TM nanoparticles was performed by drop casting of particles suspension in ethanol on a Pt foil and evaporating ethanol.

Small-angle X-ray scattering (SAXS) measurements were performed at the D02A-SAXS-2 beamline, at the Laboratorio Nacional do Luz Síncrotron (LNLS), Campinas, Brazil. The setup is equipped with a Si(111) monochromator giving a horizontally and vertically focused X-ray beam with a wavelength $\lambda = 0.161$ nm. The scattering intensity curves were measured using a CCD as a function of the modulus of the scattering vector ($q = 4 \cdot \pi / \lambda \cdot \sin(\varepsilon/2)$), with ε being the scattering angle. Samples were diluted in water and measured at room temperature in a liquid cell with mica windows as a sample holder. Data reduction was done using Fit2D package[70] and Ag-behenate was used to determine sample to detector distance (607.4(1) mm). Parasitic scattering from collimation slits was subtracted from the measured signal using the curve obtained for water in the same experimental condition.

X-ray absorption near-edge structure spectroscopy (XANES) and extended X-ray absorption fine structure (EXAFS) were employed to characterize the Au@Au(I)−TM particles. The X-ray absorption spectra were measured at the LNLS. XANES and EXAFS spectra at the Au L_3-edge (7112 eV) were recorded at XAFS-1

beamline in air at room temperature in transmission mode using a liquid cell with Kapton windows as a sample holder. Three ion chambers were employed as detectors: one before the sample to measure the incident X-ray intensity (I_0), one after the sample and before the corresponding reference metal foil to measure the intensity after the sample (I_1), and one after the metal foil (I_2). The absorption spectrum of the sample and the metal foil were expressed as $\log(I_0/I_1)$ and $\log(I_1/I_2)$, respectively. The spectrum of the metal foil was used to calibrate the absolute energy scale for the corresponding sample spectrum by positioning the absorption edge at the first inflection point. Monochromator at the SXS beamline was equipped with Si(111) crystals. XANES spectra at the sulfur K-edge were obtained in TEY mode in UHV conditions. Samples were dropped onto graphite substrate and then dried before their introduction at the main chamber.

Quantitative analysis of the results was performed by modeling and fitting the EXAFS spectra. For this purpose, structures were modeled using the FEFF code[71,59] and the EXAFS oscillation was isolated and fitted using the ATHENA and ARTEMIS programs, graphical interactive software for EXAFS analysis based on the IFEFFIT library.[72]

Transmission electron microscopy (TEM) characterization was done using a Phillips CM200 UT microscope, operating at 200 kV. Some drops of water-dispersed nanoparticles were placed on a 400 mesh ultrathin carbon type-A copper grid (Ted-Pella). The nanoparticles were dropped on the Formvar side of the grid, which is less hydrophobic than the carbon one, allowing a better distribution of the hydrophilic Au@Au(I)−TMA nanoparticles on the grid.

UV/visible spectroscopy (UV/vis) was performed with a Perkin-Elmer Lambda 35 spectrometer, equipped with a double beam. Milli-Q water was used as reference.

Supporting Information Available: UV/vis spectra of the compounds used in the synthesis, electrochemical experiments, additional TEM results, data with regards to Au(I)−TM reduction by $NaBH_4$, and results which show the stability of the particles stored as water dispersion. This material is available free of charge *via* the Internet at http://pubs.acs.org.

REFERENCES AND NOTES

1. Drechsler, U.; Erdogan, B.; Rotello, V. M. Nanoparticles: Scaffolds for Molecular Recognition. *Chem.—Eur. J.* **2004**, *10*, 5570–5579.
2. Daniel, M.; Astruc, D. Gold Nanoparticles: Assembly, Supramolecular Chemistry, Quantum-Size-Related Properties, and Applications toward Biology, Catalysis, and Nanotechnology. *Chem. Rev.* **2004**, *104*, 293–346.
3. Shenhar, R.; Rotello, V. M. Nanoparticles: Scaffolds and Building Blocks. *Acc. Chem. Res.* **2003**, *36*, 549–561.
4. Hostetler, M.; Wingate, J.; Zhong, C.; Harris, J.; Vachet, R.; Clark, M.; Londono, J.; Green, S.; Stokes, J.; Wignall, G.; *et al.* Alkanethiolate Gold Cluster Molecules with Core Diameters from 1.5 to 5.2 nm: Core and Monolayer Properties as a Function of Core Size. *Langmuir* **1998**, *14*, 17–30.

5. Leff, D. V.; Ohara, P. C.; Heath, J. R.; Gelbart, W. M. Thermodynamic Control of Gold Nanocrystal Size: Experiment and Theory. *J. Phys. Chem.* **1995**, *99*, 7036–7041.

6. Brust, M.; Walker, M.; Bethell, D.; Schiffrin, D. J.; Whyman, R. Synthesis of Thiol-Derivatised Gold Nanoparticles in a Two-Phase Liquid—Liquid System. *J. Chem. Soc., Chem. Commun.* **1994**, 801–802.

7. Boisselier, E.; Astruc, D. Gold Nanoparticles in Nanomedicine: Preparations, Imaging, Diagnostics, Therapies and Toxicity. *Chem. Soc. Rev.* **2009**, *38*, 1759–1782.

8. Jadzinsky, P. D.; Calero, G.; Ackerson, C. J.; Bushnell, D. A.; Kornberg, R. D. Structure of a Thiol Monolayer-Protected Gold Nanoparticle at 1.1 Å Resolution. *Science* **2007**, *318*, 430–433.

9. Chen, S.; Kimura, K. Synthesis and Characterization of Carboxylate-Modified Gold Nanoparticle Powders Dispersible in Water. *Langmuir* **1999**, *15*, 1075–1082.

10. Ackerson, C. J.; Jadzinsky, P. D.; Kornberg, R. D. Thiolate Ligands for Synthesis of Water-Soluble Gold Clusters. *J. Am. Chem. Soc.* **2005**, *127*, 6550–6551.

11. Brinas, R. P.; Hu, M.; Qian, L.; Lymar, E. S.; Hainfeld, J. F. Gold Nanoparticle Size Controlled by Polymeric Au(I) Thiolate Precursor Size. *J. Am. Chem. Soc.* **2008**, *130*, 975–982.

12. Templeton, A. C.; Wuelfing, W. P.; Murray, R. W. Monolayer-Protected Cluster Molecules. *Acc. Chem. Res.* **2000**, *33*, 27–36.

13. Huang, T.; Murray, R. W. Visible Luminescence of Water-Soluble Monolayer-Protected Gold Clusters. *J. Phys. Chem. B* **2001**, *105*, 12498–12502.

14. Templeton, A. C.; Chen, S.; Gross, S. M.; Murray, R. W. Water-Soluble, Isolable Gold Clusters Protected by Tiopronin and Coenzyme A Monolayers. *Langmuir* **1999**, *15*, 66–76.

15. Gies, A. P.; Hercules, D. M.; Gerdon, A. E.; Cliffel, D. E. Electrospray Mass Spectrometry Study of Tiopronin Monolayer-Protected Gold Nanoclusters. *J. Am. Chem. Soc.* **2007**, *129*, 1095–1104.

16. Schaaff, T. G.; Knight, G.; Shafigullin, M. N.; Borkman, R. F.; Whetten, R. L. Isolation and Selected Properties of a 10.4 kDa Gold:Glutathione Cluster Compound. *J. Phys. Chem. B* **1998**, *102*, 10643–10646.

17. Schaaff, T. G.; Whetten, R. L. Giant Gold-Glutathione Cluster Compounds: Intense Optical Activity in Metal-Based Transitions. *J. Phys. Chem. B* **2000**, *104*, 2630–2641.

18. Link, S.; Beeby, A.; FitzGerald, S.; El-Sayed, M. A.; Schaaff, T. G.; Whetten, R. L. Visible to Infrared Luminescence from a 28-Atom Gold Cluster. *J. Phys. Chem. B* **2002**, *106*, 3410–3415.

19. Negishi, Y.; Nobusada, K.; Tsukuda, T. Glutathione-Protected Gold Clusters Revisited: Bridging the Gap between Gold(I)—Thiolate Complexes and Thiolate-Protected Gold Nanocrystals. *J. Am. Chem. Soc.* **2005**, *127*, 5261–5270.

20. Hong, R.; Han, G.; Fernández, J. M.; Kim, B.; Forbes, N. S.; Rotello, V. M. Glutathione-Mediated Delivery and Release Using Monolayer Protected Nanoparticle Carriers. *J. Am. Chem. Soc.* **2006**, *128*, 1078–1079.

21. Gentilini, C.; Evangelista, F.; Rudolf, P.; Franchi, P.; Lucarini, M.; Pasquato, L. Water-Soluble Gold Nanoparticles Protected by Fluorinated Amphiphilic Thiolates. *J. Am. Chem. Soc.* **2008**, *130*, 15678–15682.

22. Uzun, O.; Hu, Y.; Verma, A.; Chen, S.; Centrone, A.; Stellacci, F. Water-Soluble Amphiphilic Gold Nanoparticles with Structured Ligand Shells. *Chem. Commun.* **2008**, 196–198.

23. Walter, M.; Akola, J.; Lopez-Acevedo, O.; Jadzinsky, P. D.; Calero, G.; Ackerson, C. J.; Whetten, R. L.; Grönbeck, H.; Häkkinen, H. A Unified View of Ligand-Protected Gold Clusters as Superatom Complexes. *Proc. Natl. Acad. Sci. U.S.A.* **2008**, *105*, 9157–9162.

24. Li, Y.; Galli, G.; Gygi, F. Electronic Structure of Thiolate-Covered Gold Nanoparticles: Au$_{102}$(MBA)$_{44}$. *ACS Nano* **2008**, *2*, 1896–1902.

25. Jiang, D.; Tiago, M. L.; Luo, W.; Dai, S. The "Staple" Motif: A Key to Stability of Thiolate-Protected Gold Nanoclusters. *J. Am. Chem. Soc.* **2008**, *130*, 2777–2779.

26. Vericat, C.; Vela, M. E.; Benitez, G.; Carro, P.; Salvarezza, R. C. Self-Assembled Monolayers of Thiols and Dithiols on Gold: New Challenges for a Well-Known System. *Chem. Soc. Rev.* **2010** DOI: 10.1039/b907301a.

27. Nair, A. S.; Kimura, K. Investigation of Charge Transport in Mercaptosuccinic Acid-Passivated Gold Clusters. *J. Chem. Phys.* **2008**, *129*, 184117.

28. Su, B.; Abid, J.; Fermin, D. J.; Girault, H. H.; Hoffmannova, H.; Krtil, P.; Samec, Z. Reversible Voltage-Induced Assembly of Au Nanoparticles at Liquid|Liquid Interfaces. *J. Am. Chem. Soc.* **2004**, *126*, 915–919.

29. Vasilev, K.; Zhu, T.; Glasser, G.; Knoll, W.; Kreiter, M. Preparation of Gold Nanoparticles in an Aqueous Medium Using 2-Mercaptosuccinic Acid as Both Reduction and Capping Agent. *J. Nanosci. Nanotechnol.* **2008**, *8*, 2062–2068.

30. Schaaff, T. G.; Shafigullin, M. N.; Khoury, J. T.; Vezmar, I.; Whetten, R. L.; Cullen, W. G.; First, P. N.; Gutierrez-Wing, C.; Ascensio, J.; Jose-Yacaman, M. J. Isolation of Smaller Nanocrystal Au Molecules: Robust Quantum Effects in Optical Spectra. *J. Phys. Chem. B* **1997**, *101*, 7885–7891.

31. Corbierre, M. K.; Lennox, R. B. Preparation of Thiol-Capped Gold Nanoparticles by Chemical Reduction of Soluble Au(I)—Thiolates. *Chem. Mater.* **2005**, *17*, 5691–5696.

32. van Vollenhoven, R. F. Treatment of Rheumatoid Arthritis: State of the Art 2009. *Nat. Rev. Rheumatol.* **2009**, *5*, 531–541.

33. Tiekink, E. R. T. Gold Derivatives for the Treatment of Cancer. *Crit. Rev. Oncol. Hematol.* **2002**, *42*, 225–248.

34. Hindi, K. M.; Panzner, M. J.; Tessier, C. A.; Cannon, C. L.; Youngs, W. J. The Medicinal Applications of Imidazolium Carbene—Metal Complexes. *Chem. Rev.* **2009**, *109*, 3859–3884.

35. Newman, P. M.; To, S. S.; Robinson, B. G.; Hyland, V. J.; Schrieber, L. Effect of Gold Sodium Thiomalate and Its Thiomalate Component on the *In Vitro* Expression of Endothelial Cell Adhesion Molecules. *J. Clin. Invest.* **1994**, *94*, 1864–1871.

36. Heimburger, M.; Lerner, R.; Palmblad, J. Effects of Antirheumatic Drugs on Adhesiveness of Endothelial Cells and Neutrophils. *Biochem. Pharmacol.* **1998**, *56*, 1661–1669.

37. Bratt, J.; Belcher, J.; Vercellotti, G. M.; Palmblad, J. Effects of Anti-rheumatic Gold Salts on NF-κB Mobilization and Tumour Necrosis Factor-α (TNF-α)-Induced Neutrophil-Dependent Cytotoxicity for Human Endothelial Cells. *Clin. Exp. Immunol.* **2000**, *120*, 79–84.

38. Sperling, R. A.; Gil, P. R.; Zhang, F.; Zanella, M.; Parak, W. J. Biological Applications of Gold Nanoparticles. *Chem. Soc. Rev.* **2008**, *37*, 1896–1908.

39. Brust, M.; Fink, J.; Bethell, D.; Schiffrin, D. J.; Kiely, C. Synthesis and Reactions of Functionalised Gold Nanoparticles. *J. Chem. Soc., Chem. Commun.* **1995**, 1655–1656.

40. Bourg, M.; Badia, A.; Lennox, R. B. Gold-Sulfur Bonding in 2D and 3D Self-Assembled Monolayers: XPS Characterization. *J. Phys. Chem. B* **2000**, *104*, 6562–6567.

41. Zhang, P.; Sham, T. K. X-ray Studies of the Structure and Electronic Behavior of Alkanethiolate-Capped Gold Nanoparticles: The Interplay of Size and Surface Effects. *Phys. Rev. Lett.* **2003**, *90*, 245502.

42. Tanaka, A.; Takeda, Y.; Nagasawa, T.; Takahashi, K. Chemical States of Dodecanethiolate-Passivated Au Nanoparticles: Synchrotron-Radiation Photoelectron Spectroscopy. *Solid State Commun.* **2003**, *126*, 191–196.

43. Moriarty, P. Comment on "X-ray Studies of the Structure and Electronic Behavior of Alkanethiolate-Capped Gold Nanoparticles: The Interplay of Size and Surface Effects." *Phys. Rev. Lett.* **2004**, *92*, 109601.

44. Saavedra, H. M.; Thompson, C. M.; Hohman, J. N.; Crespi,

V. H.; Weiss, P. S. Reversible Lability by *In Situ* Reaction of Self-Assembled Monolayers. *J. Am. Chem. Soc.* **2009**, *131*, 2252–2259.

45. Gelius, U; Heden, P. F; Hedman, J; Lindberg, B. J; Manne, R; Nordberg, R; Nordling, C; Siegbahn, K. Molecular Spectroscopy by Means of ESCA III. Carbon Compounds. *Phys. Scr.* **1970**, *2*, 70–80.

46. Walton, R. A. The X-ray Photoelectron Spectra of Metal Complexes of Sulfur-Containing Ligands: Sulfur 2p Binding Energies. *Coord. Chem. Rev.* **1980**, *31*, 183–220.

47. Zhong, C.; Brush, R. C.; Anderegg, J.; Porter, M. D. Organosulfur Monolayers at Gold Surfaces: Reexamination of the Case for Sulfide Adsorption and Implications to the Formation of Monolayers from Thiols and Disulfides. *Langmuir* **1999**, *15*, 518–525.

48. Vericat, C.; Benitez, G. A.; Grumelli, D. E.; Vela, M. E.; Salvarezza, R. C. Thiol-Capped Gold: From Planar to Irregular Surfaces. *J. Phys.: Condens. Matter* **2008**, *20*, 184004.

49. Schoenfisch, M. H.; Pemberton, J. E. Air Stability of Alkanethiol Self-Assembled Monolayers on Silver and Gold Surfaces. *J. Am. Chem. Soc.* **1998**, *120*, 4502–4513.

50. Vairavamurthy, A. Using X-ray Absorption to Probe Sulfur Oxidation States in Complex Molecules. *Spectrochim. Acta, Part A* **1998**, *54*, 2009–2017.

51. Ramallo-Lopez, J. M.; Giovanetti, L. J.; Requejo, F. G.; Isaacs, S. R.; Shon, Y. S.; Salmeron, M. Molecular Conformation Changes in Alkylthiol Ligands As a Function of Size in Gold Nanoparticles: X-ray Absorption Studies. *Phys. Rev. B* **2006**, *74*, 073410.

52. Zhang, P.; Sham, T. K. X-Ray Studies of the Structure and Electronic Behavior of Alkanethiolate-Capped Gold Nanoparticles: The Interplay of Size and Surface Effects. *Phys. Rev. Lett.* **2003**, *90*, 245502.

53. Zhang, P.; Sham, T. K. Fabrication of Thiol-Capped Pd Nanoparticles: An Electrochemical Method. *Appl. Phys. Lett.* **2003**, *82*, 1778.

54. Baker, T. A.; Friend, C. M.; Kaxiras, E. Atomic Oxygen Adsorption on Au(111) Surfaces with Defects. *J. Phys. Chem. C* **2009**, *113*, 3232–3238.

55. Jones, P. G.; Rumpel, H.; Schwarzmann, E.; Sheldrick, G. M.; Paulus, H. Gold(III) Oxide. *Acta Crystallogr., Sect. B* **1979**, *35*, 1435–1437.

56. Bau, R. Crystal Structure of the Antiarthritic Drug Gold Thiomalate (Myochrysine): A Double-Helical Geometry in the Solid State. *J. Am. Chem. Soc.* **1998**, *120*, 9380–9381.

57. Elder, R. C.; Ludwig, K.; Cooper, J. N.; Eidsness, M. K. EXAFS and WAXS Structure Determination for an Antiarthritic Drug, Sodium Gold(I) Thiomalate. *J. Am. Chem. Soc.* **1985**, *107*, 5024–5025.

58. Mazid, M. A.; Razi, M. T.; Sadler, P. J.; Greaves, G. N.; Gurman, S. J.; Koch, M. H. J.; Phillips, J. C. An EXAFS Study of Gold Co-ordination in the Anti-arthritic Drugs Myocrisin and Solganol. *J. Chem. Soc., Chem. Commun.* **1980**, 1261–1263.

59. Menard, L. D.; Xu, H.; Gao, S.; Twesten, R. D.; Harper, A. S.; Song, Y.; Wang, G.; Douglas, A. D.; Yang, J. C.; Frenkel, A. I.; *et al.* Metal Core Bonding Motifs of Monodisperse Icosahedral Au13 and Larger Au Monolayer-Protected Clusters As Revealed by X-ray Absorption Spectroscopy and Transmission Electron Microscopy. *J. Phys. Chem. B* **2006**, *110*, 14564–14573.

60. de Graaf, J; van Dillen, A. J; de Jong, K. P; Koningsberger, D. C. Preparation of Highly Dispersed Pt Particles in Zeolite Y with a Narrow Particle Size Distribution: Characterization by Hydrogen Chemisorption, TEM, EXAFS Spectroscopy, and Particle Modeling. *J. Catal.* **2001**, *203*, 307–321.

61. Ramallo-López, J.; Requejo, F.; Craievich, A.; Wei, J.; Avalos-Borja, M.; Iglesia, E. Complementary Methods for Cluster Size Distribution Measurements: Supported Platinum Nanoclusters in Methane Reforming Catalysts. *J. Mol. Catal. A* **2005**, *228*, 299–307.

62. Garzón, I. L.; Rovira, C.; Michaelian, K.; Beltrán, M. R.; Ordejón, P.; Junquera, J.; Sánchez-Portal, D.; Artacho, E.; Soler, J. M. Do Thiols Merely Passivate Gold Nanoclusters? *Phys. Rev. Lett.* **2000**, *85*, 5250.

63. Söderlund, J.; Kiss, L. B.; Niklasson, G. A.; Granqvist, C. G. Lognormal Size Distributions in Particle Growth Processes without Coagulation. *Phys. Rev. Lett.* **1998**, *80*, 2386.

64. Kim, J; Cha, S; Shin, K; Jho, J. Y; Lee, J. Synthesis of Gold Nanoparticles from Gold(I)−Alkanethiolate Complexes with Supramolecular Structures through Electron Beam Irradiation in TEM. *J. Am. Chem. Soc.* **2005**, *127*, 9962–9963.

65. Yao, H.; Kojima, H.; Sato, S.; Kimura, K. Interparticle Spacing Control in the Superlattices of Carboxylic Acid-Capped Gold Nanoparticles by Hydrogen-Bonding Mediation. *Langmuir* **2004**, *20*, 10317–10323.

66. Ristau, R.; Tiruvalam, R.; Clasen, P. L.; Gorskowski, E. P.; Harmer, M. P.; Kiely, C. J.; Hussain, I.; Brust, M. Electron Microscopy Studies of the Thermal Stability of Gold Nanoparticle Arrays. *Gold Bull.* **2009**, *42*, 133–143.

67. Shon, Y.; Mazzitelli, C.; Murray, R. W. Unsymmetrical Disulfides and Thiol Mixtures Produce Different Mixed Monolayer-Protected Gold Clusters. *Langmuir* **2001**, *17*, 7735–7741.

68. Bau, R. Crystal Structure of the Antiarthritic Drug Gold Thiomalate (Myochrysine): A Double-Helical Geometry in the Solid State. *J. Am. Chem. Soc.* **1998**, *120*, 9380–9381.

69. Block, B. P. Gold Powder and Potassium Tetrabromoaurate (III). *Inorg. Synth.* **1953**, *4*, 14–17.

70. http://www.esrf.eu/computing/scientific/FIT2D/.

71. Zabinsky, S. I.; Rehr, J. J.; Ankudinov, A.; Albers, R. C.; Eller, M. J. Multiple-Scattering Calculations of X-Ray-Absorption Spectra. *Phys. Rev. B* **1995**, *52*, 2995–3009.

72. Ravel, B; Newville, M. ATHENA, ARTEMIS, HEPHAESTUS: Data Analysis for X-Ray Absorption Spectroscopy Using IFEFFIT. *J. Synchrotron Radiat.* **2005**, *12*, 537–541.